

Supporting Information

Grape juice: an effective liquid additive for significant enhancement of thermoelectric performance in Cu₂Se

Sheik Md Kazi Nazrul Islam ^{ac}, Michael B. Cortie ^c, and Xiaolin Wang ^{*ab}

* Corresponding author

^a Institute for Superconducting and Electronic Materials, Australian Institute for Innovative Materials, University of Wollongong, North Wollongong, NSW 2500, Australia, E-mail: xiaolin@uow.edu.au

^b ARC Centre of Excellence in Future Low-Energy Electronics Technologies, University of Wollongong, Australia

^c School of Mathematical and Physical Sciences, University of Technology Sydney, Broadway, NSW 2007, Australia

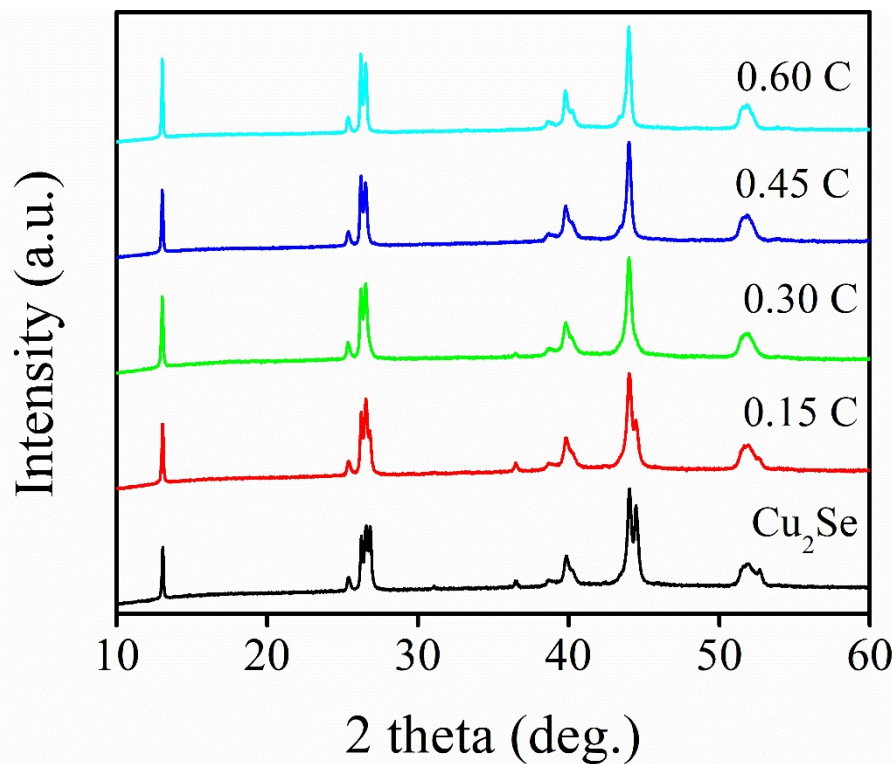


Figure S1 Room temperature X-ray diffraction patterns of pure Cu₂Se and carbon-incorporated Cu₂Se ($Cu_2Se - x \text{ wt.\% } C$ samples ($x = 0, 0.15, 0.30, 0.45, \text{ and } 0.60$)). The patterns match with the room temperature Cu₂Se with the PDF number 47-1448. With increasing carbon concentration there is a gradual decrease in the peak intensity at 36.50°, shoulder peaks at 26.84°, 44.46°, and 52.65° (2-theta).

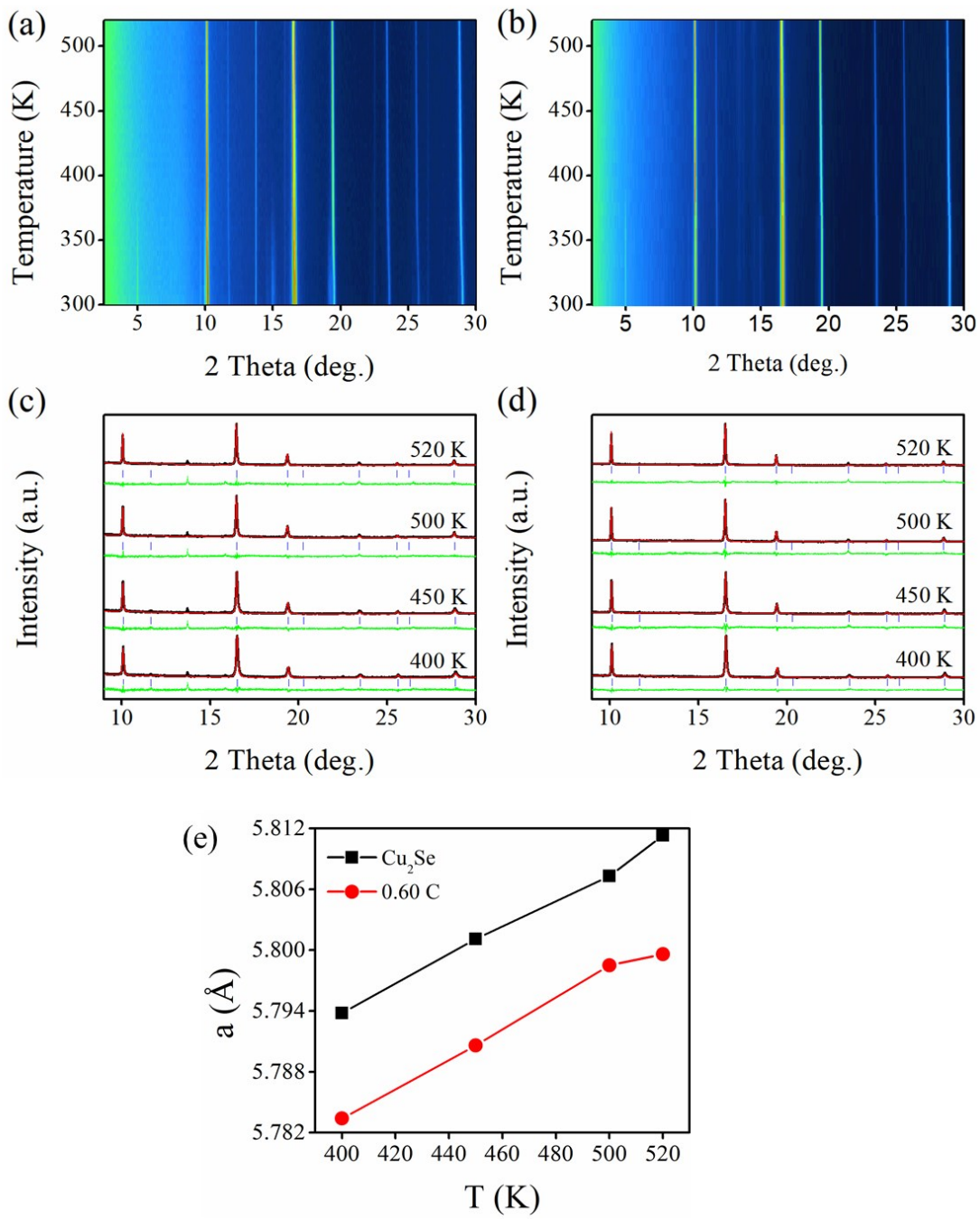


Figure S2 (a, b) Synchrotron X-ray diffraction profiles of pure Cu₂Se and 0.60 wt.% C - incorporated Cu₂Se obtained upon heating, showing the disappearance of the extra peaks around 5° and 15° due to the transformation of monoclinic α -phase to the cubic β -phase. (c, d) Rietveld refinement XRD patterns for the unincorporated and 0.6 wt.% C - incorporated Cu₂Se samples, respectively; (e) Change in lattice parameters of the β -phase for unincorporated and 0.6 wt.% C - incorporated samples. The refined parameters are shown in Table S1.

Table S1 | Lattice parameters, R-factors for the pure Cu₂Se and 0.6 wt.% carbon-incorporated Cu₂Se at different temperatures.

Temp (K)	Lattice parameter Sample	a (Å)	R _p	R _{wp}	χ^2
520	0.6 wt.% C	5.79960	8.800	11.667	1.788
500	0.6 wt.% C	5.79850	8.379	11.279	1.664
450	0.6 wt.% C	5.79060	8.439	11.160	1.648
400	0.6 wt.% C	5.78340	8.731	11.404	1.728
520	Cu ₂ Se	5.81130	8.031	11.066	1.840
500	Cu ₂ Se	5.80730	8.081	10.908	1.790
450	Cu ₂ Se	5.80110	7.897	10.640	1.753
400	Cu ₂ Se	5.79380	7.745	10.351	1.704

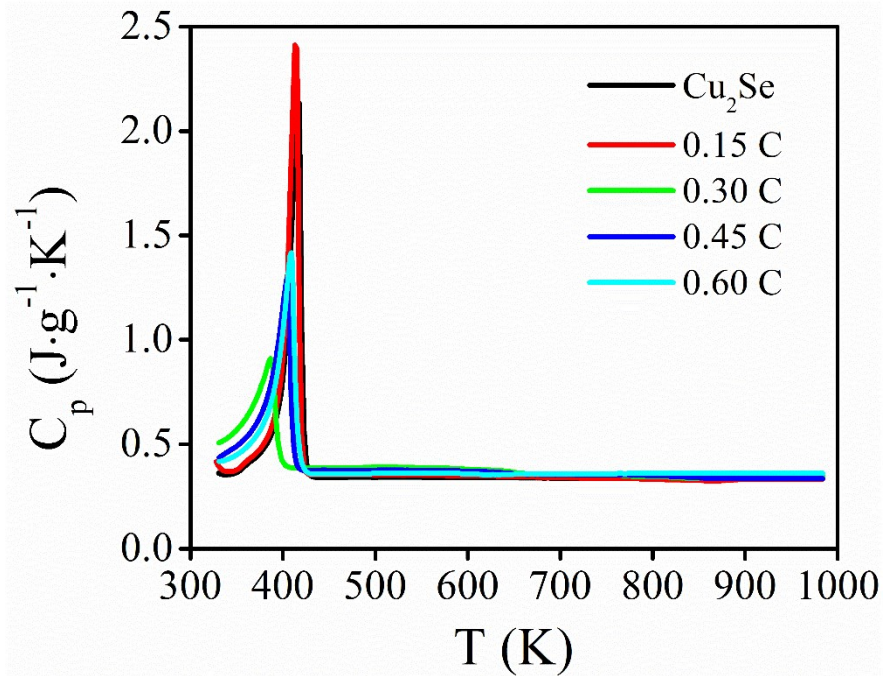


Figure S3. Temperature-dependence heat capacity (C_p) for different concentrations of carbon in Cu₂Se.

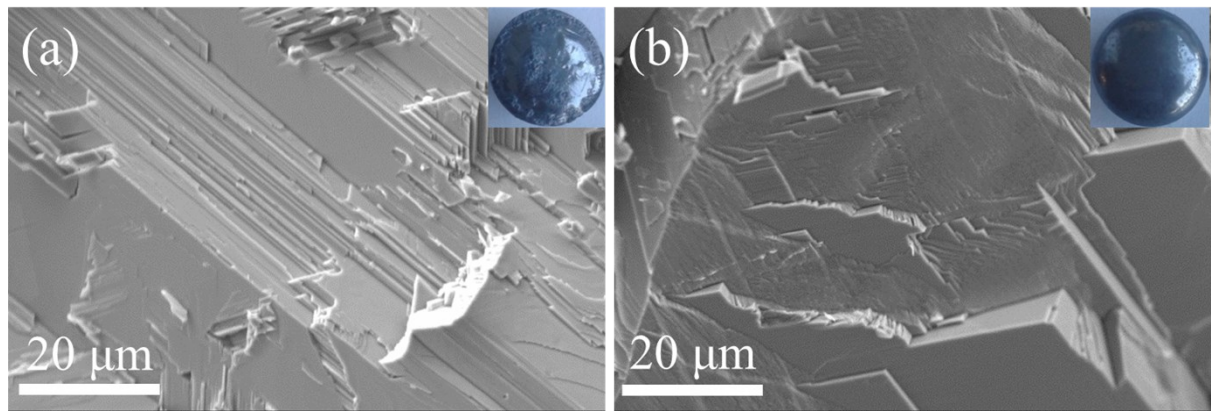


Figure S4. FE-SEM fracture surfaces of the (a) pure and (b) 0.6 wt.% C-incorporated Cu₂Se polycrystalline samples (inset- as-prepared droplet).

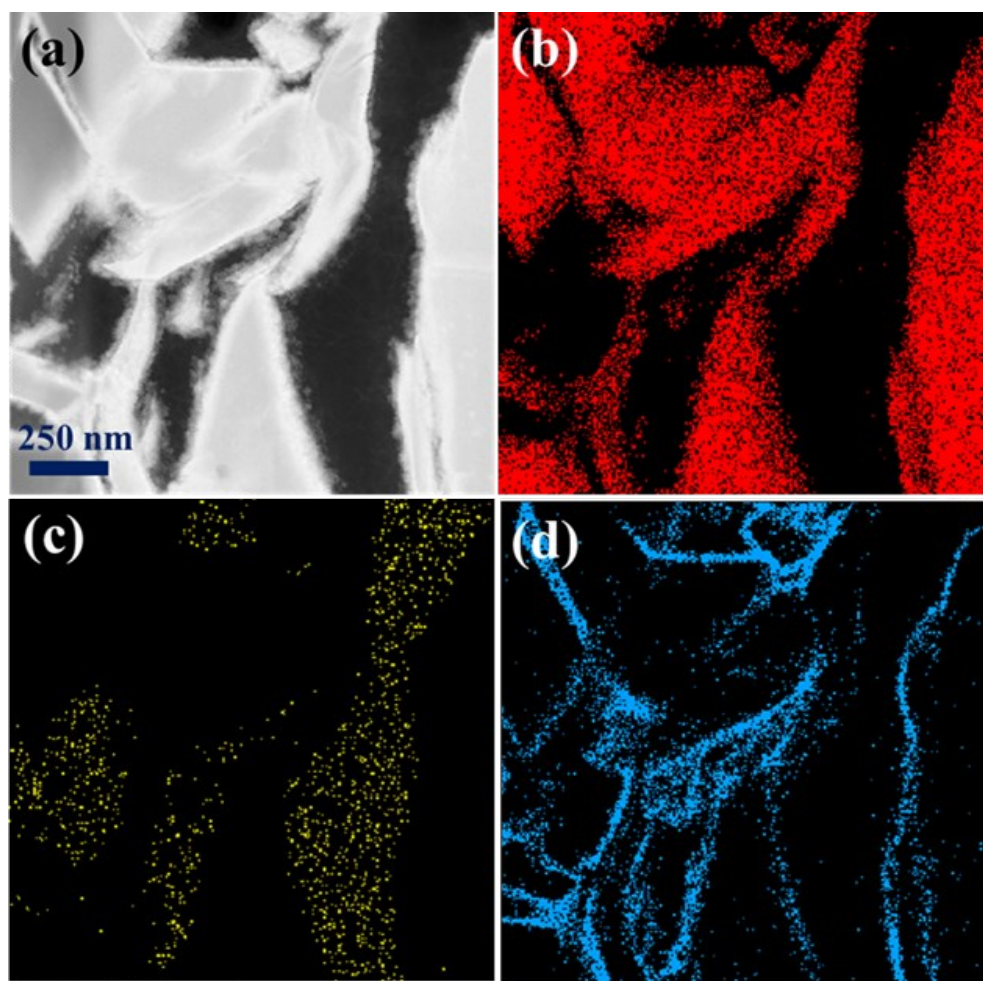


Figure S5. STEM micrograph of a 0.60 wt.% C-incorporated Cu₂Se sample. (a) Low magnification TEM image used for phase analysis using EDS mapping; (b) Cu₂Se phase; (c) C phase; (d) Cu₂O Phase

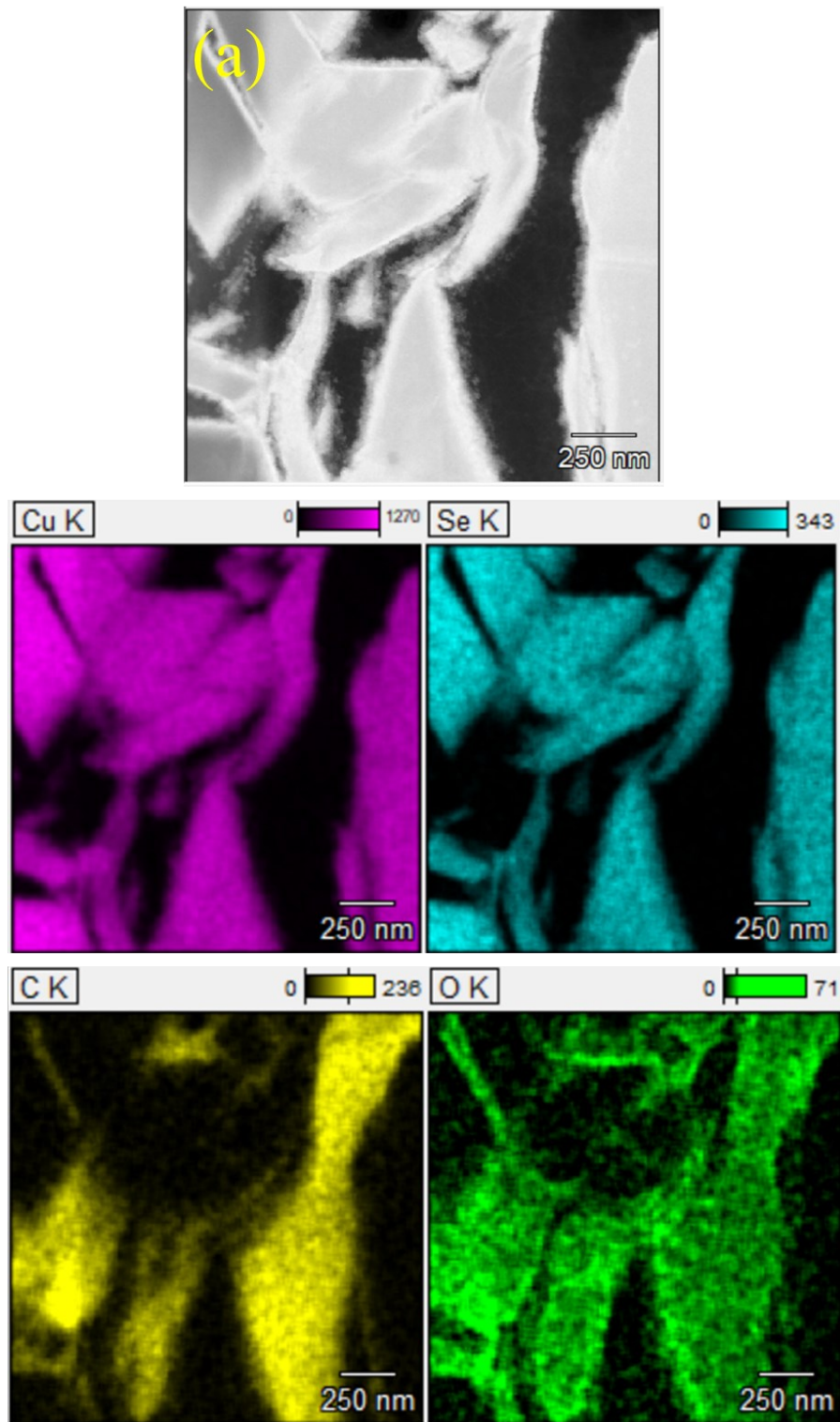


Figure S6. (a) STEM image of the 0.60 wt.% carbon incorporated Cu₂Se composites and the corresponding EDS elemental mapping of Cu, Se, C and O.

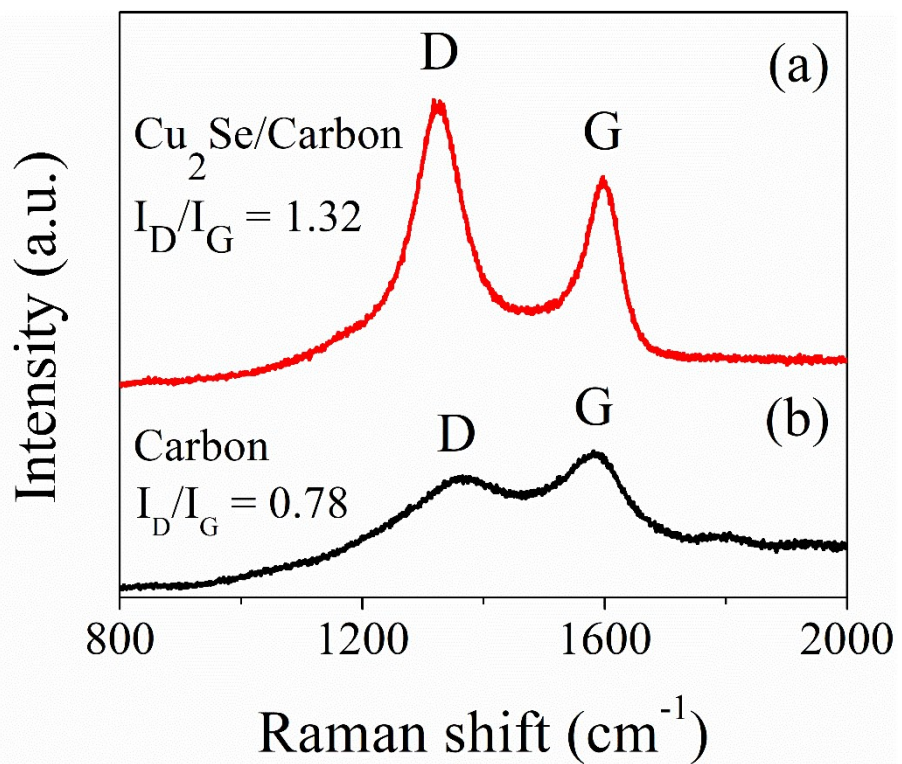


Figure S7. Raman spectra of the (a) 0.60 wt.% C-incorporated Cu₂Se sample and (b) pure carbon extracted by pyrolyzing grape juice to 200 °C, showing the main Raman features, the D, and G bands, taken with a laser wavelength of 636 nm.

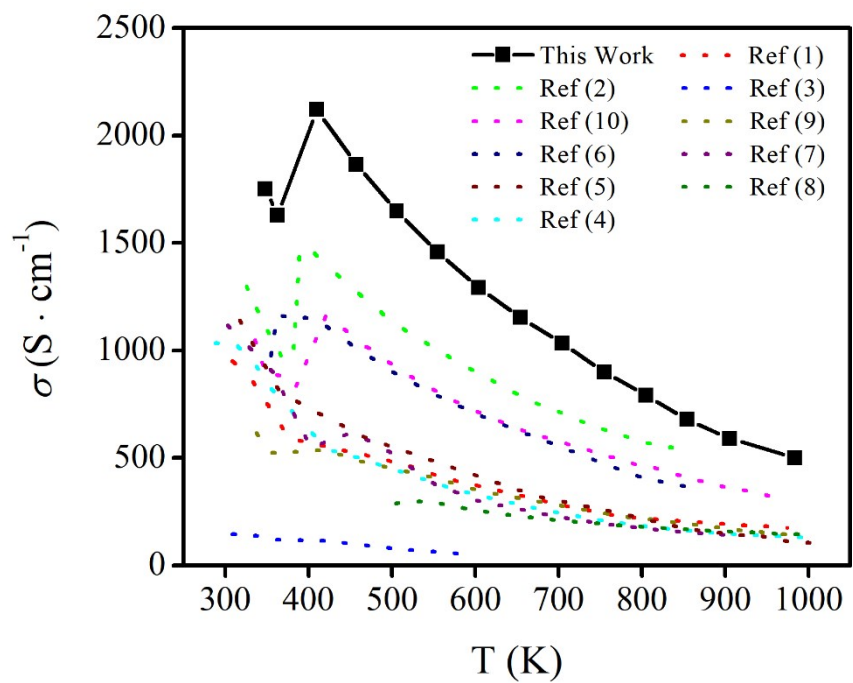


Figure S8. Comparison of the electrical conductivity of 0.30 wt.% C-incorporated Cu_2Se sample as a function of temperature (dotted lines show data for state-of-the-art Cu_2Se polycrystals from the literature.¹⁻¹⁰⁾

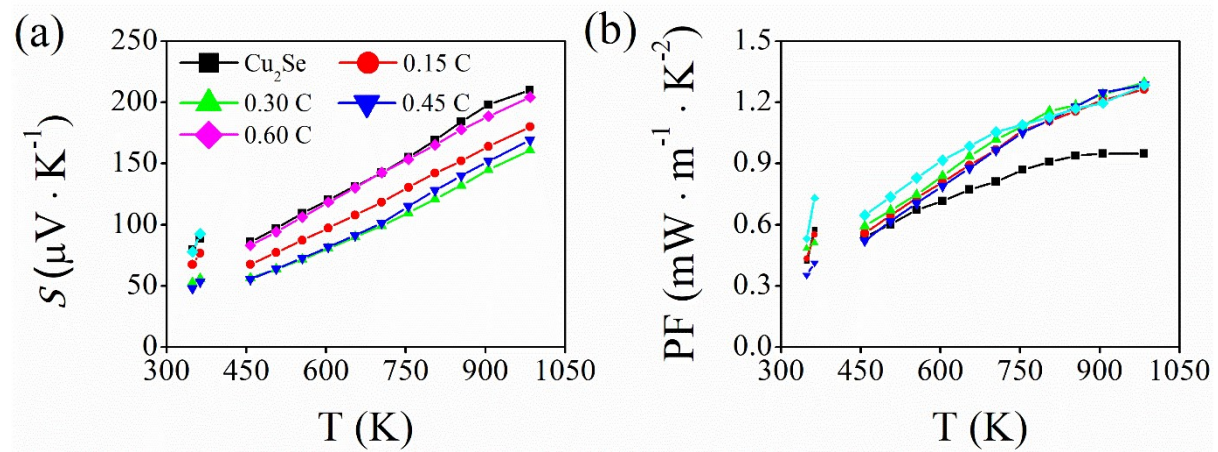


Figure S9. Temperature-dependence of (a) Seebeck coefficient (S); (b) power factor (PF) for different concentrations of carbon in Cu_2Se .

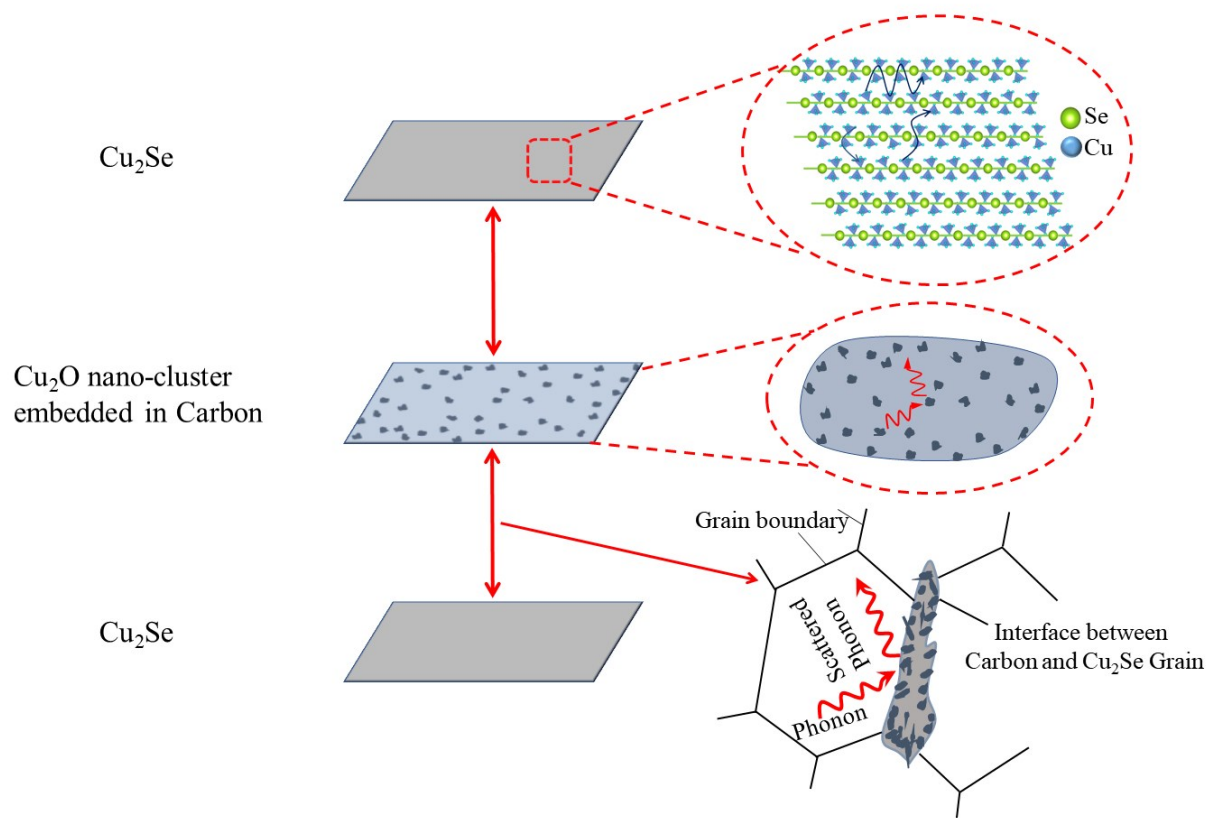


Figure S10. Schematic diagram of phonon transport mechanism in $\text{Cu}_2\text{Se}^{10}$, Cu_2O nanocluster embedded in interface between carbon and Cu_2Se grain.

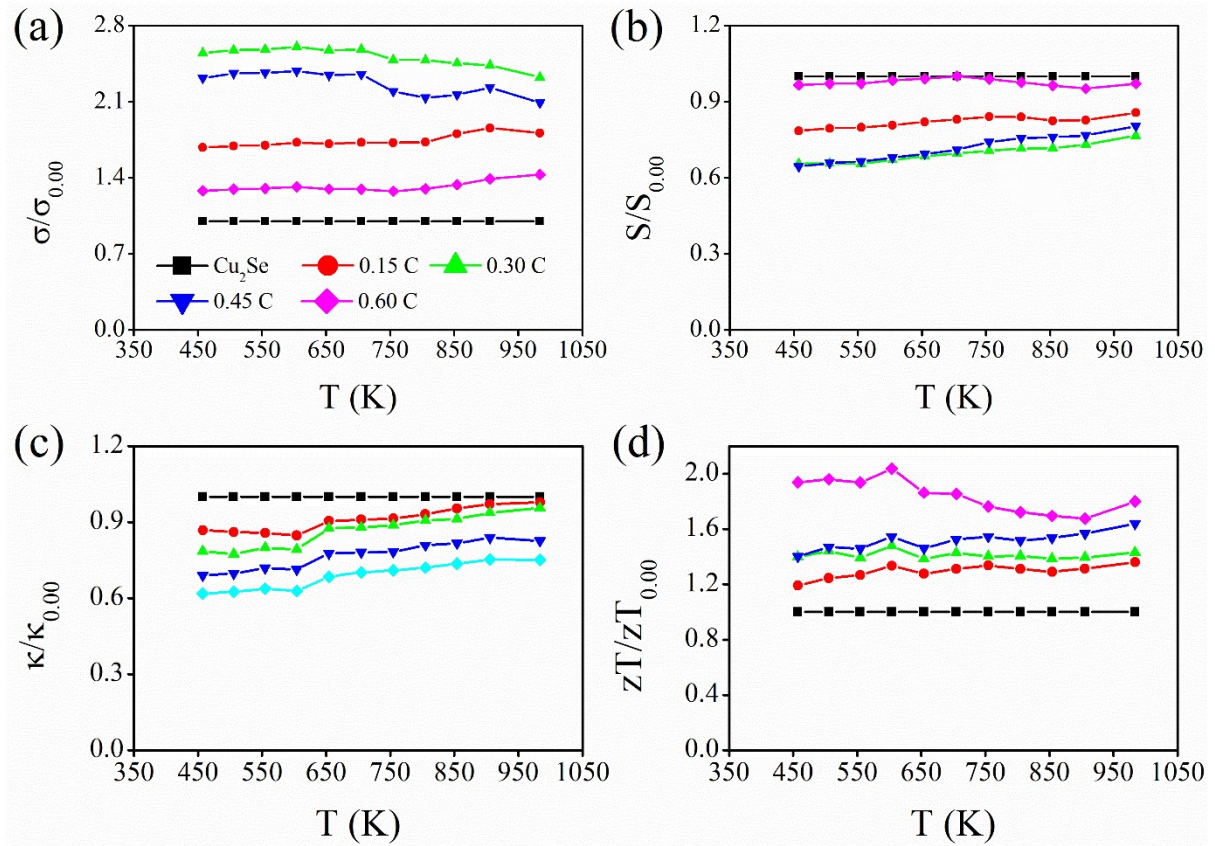


Figure S11. Temperature dependence of (a) $\sigma/\sigma_{0.00}$, (b) $S/S_{0.00}$, (c) $\kappa/\kappa_{0.00}$, and (d) $zT/zT_{0.00}$ for the carbon incorporated Cu₂Se samples with doping levels of 0.15, 0.30, 0.45 and 0.60 wt.%.

References

1. B. Gahtori, S. Bathula, K. Tyagi, M. Jayasimhadri, A. Srivastava, S. Singh, R. Budhani and A. Dhar, *Nano Energy*, 2015, **13**, 36-46.
2. A. Olvera, N. Moroz, P. Sahoo, P. Ren, T. Bailey, A. Page, C. Uher and P. Poudeu, *Energy & Environmental Science*, 2017, **10**, 1668-1676.
3. T. W. Day, K. S. Weldert, W. G. Zeier, B.-R. Chen, S. L. Moffitt, U. Weis, K. P. Jochum, M. Panthöfer, M. J. Bedzyk and G. J. Snyder, *Chemistry of Materials*, 2015, **27**, 7018-7027.
4. L. Zhao, X. Wang, F. F. Yun, J. Wang, Z. Cheng, S. Dou, J. Wang and G. J. Snyder, *Adv. Electron. Mater.*, 2015, **1**, 1400015.
5. L.-l. Zhao, X.-l. Wang, J.-y. Wang, Z.-x. Cheng, S.-x. Dou, J. Wang and L.-q. Liu, *Scientific reports*, 2015, **5**, 7671.
6. L. Zhao, S. M. K. N. Islam, J. Wang, D. L. Cortie, X. Wang, Z. Cheng, J. Wang, N. Ye, S. Dou, X. Shi, L. Chen, G. J. Snyder and X. Wang, *Nano Energy*, 2017, **41**, 164-171.
7. M. Y. Tafti, S. Ballikaya, A. M. Khachatourian, M. Noroozi, M. Saleemi, L. Han, N. V. Nong, T. Bailey, C. Uher and M. S. Toprak, *Rsc Advances*, 2016, **6**, 111457-111464.
8. B. Zhong, Y. Zhang, W. Li, Z. Chen, J. Cui, W. Li, Y. Xie, Q. Hao and Q. He, *Applied Physics Letters*, 2014, **105**, 123902.
9. S. D. Kang, J.-H. Pöhls, U. Aydemir, P. Qiu, C. C. Stoumpos, R. Hanus, M. A. White, X. Shi, L. Chen and M. G. Kanatzidis, *Materials Today Physics*, 2017, **1**, 7-13.
10. H. Liu, X. Shi, F. Xu, L. Zhang, W. Zhang, L. Chen, Q. Li, C. Uher, T. Day and G. J. Snyder, *Nature materials*, 2012, **11**, 422-425.
11. S. Ballikaya, H. Chi, J. R. Salvador and C. Uher, *Journal of Materials Chemistry A*, 2013, **1**, 12478-12484.
12. G. Tan, F. Shi, S. Hao, L.-D. Zhao, H. Chi, X. Zhang, C. Uher, C. Wolverton, V. P. Dravid and M. G. Kanatzidis, *Nature communications*, 2016, **7**, 12167.